J|A|C|S

A R T I C L E S

Meta Conjugation Effect on the Torsional Motion of Aminostilbenes in the Photoinduced Intramolecular Charge-Transfer State

Jye-Shane Yang,*,† Kang-Ling Liau,‡ Chun-Yi Li,† and Mon-Yao Chen‡

Department of Chemistry, National Taiwan University, Taipei, Taiwan 10617 and Department of Chemistry, National Central University, Chungli, Taiwan 32054

Received June 6, 2007; E-mail: jsyang@ntu.edu.tw

Abstract: The photochemical behavior of a series of *trans*-3-(*N*-arylamino)stilbenes (**m1**, aryl = 4-substituted phenyl with a substituent of cyano (**CN**), hydrogen (**H**), methyl (**Me**), or methoxy (**OM**)) in both nonpolar and polar solvents is reported and compared to that of the corresponding para isomers (**p1CN**, **p1H**, **p1Me**, and **p1OM**). The distinct propensity of torsional motion toward a low-lying twisted intramolecular charge-transfer (TICT) state from the planar ICT (PICT) precursor between the meta and para isomers of **1CN** and **1Me** reveals the intriguing meta conjugation effect and the importance of the reaction kinetics. Whereas the poor charge-redistribution (delocalization) ability through the *meta*-phenylene bridge accounts for the unfavorable TICT-forming process for **m1CN**, it is such a property that slows down the decay processes of fluorescence and photoisomerization for **m1Me**, facilitating the competition of the single-bond torsional reaction. In contrast, the quinoidal character for **p1Me** in the PICT state kinetically favors both fluorescence and photoisomerization but disfavors the single-bond torsion. The resulting concept of thermodynamically allowed but kinetically inhibited TICT formation could also apply to understanding the other D−A systems, including *trans*-4-cyano-4′-(*N*,*N*-dimethylamino)stilbene (DCS) and 3-(*N*,*N*-dimethylamino)benzonitrile (3DMABN).

Introduction

The electronic properties such as photoluminescence, energy migration, electron transfer, conductivity, and nonlinear optics for a π-conjugated system strongly depend on the degree of electronic coupling (delocalization) between the subunits.[1−8] It is well known that electronic coupling through a *meta*-phenylene

(*m*-Ph) bridge is inherently weaker than through a *para*-phenylene (*p*-Ph) one.[1,2] However, recent studies have shown that their difference becomes smaller on going from the ground to the excited state,[3] and the meta conjugation effect could be further enhanced by structural modifications on the Ph bridge (e.g., replaced by pyridyl or phenol groups)[4,5] or the subunits (e.g., presence of electron-donating amino or alkoxy groups).[6] Such a state- and structure-dependent meta conjugation effect could be a merit for designing new organic materials. Indeed, it has recently been revealed that meta-bridged electron donor−acceptor (D−A) systems are potential candidates as high-efficiency solar-cell sensitizers because upon electronic excitation the meta bridge allows efficient intramolecular charge transfer (ICT) for the desired charge-separation but not for the unwanted charge-recombination processes.[7]

Another crucial factor that determines the degree of electronic coupling in π-conjugated systems is the conformation: namely, the more planar the molecular structure, the stronger the coupling. While electronic excitation generally planarizes the system and thus increases the charge-delocalization (mesomeric) interactions,[9] discrepancies have been found for some D−A systems, which undergo torsional motion about the D−A bond and lead to a charge-separated twisted ICT (TICT) state (Figure

† National Taiwan University.
‡ National Central University.

(1) (a) Karabunarliev, S.; Baumgarten, M.; Tyutyulkov, N.; Müllen, K. *J. Phys. Chem.* **1994**, *98*, 11892−11901. (b) Tammer, M.; Horsburgh, L.; Monkman, A. P.; Brown, W.; Burrows, H. D. *Adv. Funct. Mater.* **2002**, *12*, 447−454. (c) Chu, Q.; Pang, Y.; Ding, L.; Karasz, F. E. *Macromolecules* **2002**, *35*, 7569−7574. (d) Oliva, M. M.; Casado, J.; Hennrich, G.; Navarrete, J. T. L. *J. Phys. Chem. B* **2006**, *110*, 19198−19206.
(2) (a) Hong, S. Y.; Kim, D. Y.; Kim, C. Y.; Hoffmann, R. *Macromolecules* **2001**, *34*, 6474−6481. (b) Pogantsch, A.; Mahler, A. K.; Hayn, C.; Saf, R.; Stelzer, F.; List, E. J. W.; Brédas, J.-L.; Zojer, E. *Chem. Phys.* **2004**, *297*, 143−151. (c) Yang, J.-S.; Lee, Y.-R.; Yan, J.-L.; Lu, M.-C. *Org. Lett.* **2006**, *8*, 5813−5816.
(3) (a) Díez-Barra, E.; García-Martínez, J. C.; Merino, S.; del Rey, R.; Rodríguez-López, J.; Sánchez-Verdú, P.; Tejeda, J. *J. Org. Chem.* **2001**, *66*, 5664−5670. (b) Gaab, K. M.; Thompson, A. L.; Xu, J.; Martinez, T. J.; Bardeen, C. J. *J. Am. Chem. Soc.* **2003**, *125*, 9288−9289. (c) Thompson, A. L.; Gaab, K. M.; Xu, J.; Bardeen, C. J.; Martinez, T. J. *J. Phys. Chem. A* **2004**, *108*, 671−682. (d) Ranasinghe, M. I.; Hager, M. W.; Gorman, C. B.; Goodson, T., III *J. Phys. Chem. B* **2004**, *108*, 8543−8549.
(4) Song, C.; Swager, T. M. *Macromolecules* **2005**, *38*, 4569−4576.
(5) (a) Yamaguchi, Y.; Kobayashi, S.; Wakamiya, T.; Matsubara, Y.; Yoshida, Z. *Angew. Chem., Int. Ed.* **2005**, *44*, 7040−7044. (b) Priego, E. M.; Sánchez, L.; Herranz, M. A.; Martín, N.; Viruela, R.; Ortí, E. *Org. Biomol. Chem.* **2007**, *5*, 1201−1209.
(6) (a) Bangal, P. R.; Lam, D. M. K.; Peteanu, L. A.; Van der Auweraer, M. *J. Phys. Chem. B* **2004**, *108*, 16834−16840. (b) Yamaguchi, Y.; Ochi, T.; Miyamura, S.; Tanaka, T.; Kobayashi, S.; Wakamiya, T.; Matsubara, Y.; Yoshida, Z. *J. Am. Chem. Soc.* **2006**, *128*, 4504−4505.
(7) Thompson, A. L.; Ahn, T.-S.; Thomas, K. R. J.; Thayumanavan, S.; Martinez, T. J.; Bardeen, C. J. *J. Am. Chem. Soc.* **2005**, *127*, 16348−16349.

(8) (a) Peng, Z.; Pan, Y.; Xu, B.; Zhang, J. *J. Am. Chem. Soc.* **2000**, *122*, 6619−6623. (b) Melinger, J. S.; Pan, Y.; Kleiman, V. D.; Peng, Z.; Davis, B. L.; McMorrow, D.; Lu, M. *J. Am. Chem. Soc.* **2002**, *124*, 12002−12012. (c) Pan, Y.; Lu, M.; Peng, Z.; Melinger, J. S. *J. Org. Chem.* **2003**, *68*, 6952−6958. (d) Tomonari, M.; Ookubo, N. *Chem. Phys. Lett.* **2003**, *376*, 504−514.
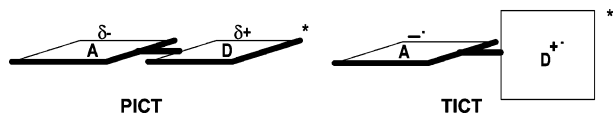
Figure 1. Schematic drawing of geometries and electronic character for the PICT and TICT states of electron donor (D)−acceptor (A) conjugated systems.

1).[10,11] The driving force for the TICT state formation is to increase the dipole moment and thus gain better solvation in polar solvents. The TICT concept originated from the interpretation of the dual fluorescence behavior of 4-(*N,N*-dimethylami-no)benzonitrile (DMABN) in polar solvents.[12] The proposed TICT state is a successor of the so-called locally excited (LE) state through the twisting of the C_{ph}–N bond. Because of the forbidden nature in optical transition for the charge-recombination process, the TICT state is characterized with low fluorescence quantum efficiency. However, such an argument has been challenged by several other alternative models, and the most important one is the planar ICT (PICT) state.[13,14] Recent progress on this issue has revealed that dual fluorescence could result from the LE−PICT or the PICT−TICT as well as the LE−TICT states, depending on the molecular structures.[15] TICT-based dual fluorescent systems have been applied in the design of ratiometric fluorescent chemosensors.[16] In addition, the TICT concept has inspired the design of ground-state twisted zwitterionic D−A systems of ultralarge hyperpolarizability.[17]

DMABN   3DMABN   DCS
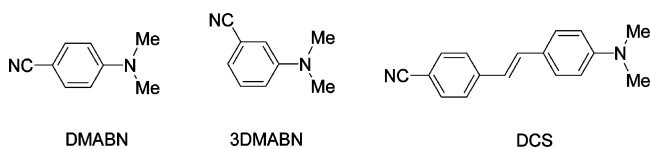
Despite the numerous investigations of the ICT behavior of D−A systems, to predict whether a TICT state is formed simply based on the molecular structure remains to be a challenging task. For example, the meta isomer of DMABN (i.e., 3DMABN)

displays an anti-TICT behavior (e.g., nondual fluorescence and large fluorescence quantum yields),[14,18] although its TICT state was expected to be lower in energy than the LE state.[14,19] Likewise, the π-elongated DMABN analog *trans*-4-cyano-4′-(*N,N*-dimethylamino)stilbene (DCS) was computationally predicted to possess a low-lying TICT state,[20] but many experimental studies have shown it to be a TICT-free species.[21−23] While such discrepancies have been employed to argue against the validity of the TICT model,[14,21,22] an alternative explanation is the unfavorable reaction kinetics. In other words, a low-lying TICT state (i.e., thermodynamically favorable) might not guarantee its formation unless the process of the torsional motion is also sufficiently fast to compete with the other decay channels. However, addressing the TICT kinetics for a D−A system is by no means straightforward. This is evidenced by the fact that even for the prototype DMABN molecule the reaction mechanism is still under discussion.[11,24,25] For example, a torsional barrier is present in the conventional adiabatic precursor (LE)−successor (TICT) model,[11] but it has recently been shown that the TICT state can be formed directly from the Franck−Condon (FC) state on S_2 through a conical intersection, corresponding to a nonadiabatic and nearly barrierless reaction route.[11,26,27] The situation is even worse in TICT-free systems because experimental evaluation of the kinetic factors for a hypothetical torsional process is impossible. While theoretical modeling in search of the transition state and thus the reaction barrier might provide a solution, reliable computational methods remain to be established. As a result, the absence of TICT state formation is often intuitively attributed to a high-lying TICT state (e.g., 3DMABN[18]), and to date, the concept of thermodynamically allowed (i.e., exothermic) but kinetically inhibited (i.e., slow) D−A torsional motion has not yet been demonstrated.

trans-Aminostilbenes, including DCS, are a special category of D−A molecules that could undergo another type of torsional motion in the photoinduced ICT states: namely, the central double-bond torsion that leads to trans−cis photoisomerization.

(9) For examples, see: (a) Sluch, M. I.; Godt, A.; Bunz, U. H. F.; Berg, M. A. *J. Am. Chem. Soc.* **2001**, *123*, 6447−6448. (b) Yang, J.-S.; Yan, J.-L.; Hwang, C.-Y.; Chiou, S.-Y.; Liau, K.-L.; Tsai, H.-S. G.; Lee, G.-Hs.; Peng, S.-M. *J. Am. Chem. Soc.* **2006**, *128*, 14109−14119.
(10) (a) Rettig, W. *Angew. Chem., Int. Ed. Engl.* **1986**, *25*, 971−988. (b) Rettig, W.; Maus, M. *Conformational Analysis of Molecules in Excited States*; Waluk, J., Ed.; Wiley-VCH: New York, 2000; Chapter 1, pp 1−55.
(11) Grabowski, Z. R.; Rotkiewicz, K. *Chem. Rev.* **2003**, *103*, 3899−4031.
(12) (a) Lippert, E.; Lüder, W.; Moll, F.; Nägle, W.; Boos, H.; Prigge, H.; Seibold-Blankenstein, I. *Angew. Chem.* **1961**, *73*, 695−706. (b) Lippert, E.; Lüder, W.; Boos, H. In *Advances in Molecular Spectroscopy*; Mangini, A., Ed.; Pergamon Press: Oxford, 1962; pp 443−457.
(13) (a) von der Haar, T.; Hebecker, A.; Il'ichev, Y. V.; Jiang, Y.-B.; Kühnle, W.; Zachariasse, K. A. *Recl. Trav. Chim. Pays-Bas* **1995**, *114*, 430−442. (b) Zachariasse, K. A.; Grobys, M.; von der Haar, T.; Hebecker, A.; Il'ichev, Y. V.; Jiang, Y.-B.; Morawski, O.; Kühnle, W. *J. Photochem. Photobiol. A: Chem.* **1996**, *102*, 59−70. (c) Zachariasse, K. A.; Grobys, M.; von der Haar, T.; Hebecker, A.; Il'ichev, Y. V.; Morawski, O.; Rückert, I.; Kühnle, W. *J. Photochem. Photobiol. A: Chem.* **1997**, *105*, 373−383. (d) Il'ichev, Y. V.; Kühnle, W.; Zachariasse, K. A. *J. Phys. Chem.* **1998**, *102*, 5670−5680. (e) Demeter, A.; Zachariasse, K. A. *Chem. Phys. Lett.* **2003**, *380*, 699−703. (f) Zachariasse, K. A.; Druzhinin, S. I.; Bosch, W.; Machinek, R. *J. Am. Chem. Soc.* **2004**, *126*, 1705−1715. (g) Techert, S.; Zachariasse, K. A. *J. Am. Chem. Soc.* **2004**, *126*, 5593−5600.
(14) (a) Zachariasse, K.; van der Haar, T.; Hebecker, A.; Leinhos, U.; Kühnle, W. *Pure Appl. Chem.* **1993**, *65*, 1745−1750. (b) Zachariasse, K. A. *Chem. Phys. Lett.* **2000**, *320*, 8−13.
(15) Cogan, S.; Zilberg, S.; Haas, Y. *J. Am. Chem. Soc.* **2006**, *128*, 3335−3345.
(16) (a) Létard, J.-F.; Delmond, S.; Lapouyade, R.; Braun, D.; Rettig, W.; Kreissler, M. *Recl. Trav. Chim. Pays-Bas* **1995**, *114*, 517−527. (b) Collins, G. E.; Choi, L.-S.; Callahan, J. H. *J. Am. Chem. Soc.* **1998**, *120*, 1474−1478. (c) Aoki, S.; Kagata, D.; Shiro, M.; Takeda, K.; Kimura, E. *J. Am. Chem. Soc.* **2004**, *126*, 13377−13390. (d) Liu, B.; Chen, J.; Yang, G.; Li, Y. *Res. Chem. Intermed.* **2004**, *30*, 345−353. (e) Yang, J.-S.; Hwang, C.-Y.; Chen, M.-Y. *Tetrahedron Lett.* **2007**, *48*, 3097−3102.
(17) (a) Albert, I. D. L.; Marks, T. J.; Ratner, M. A. *J. Am. Chem. Soc.* **1997**, *119*, 3155−3156. (b) Albert, I. D. L.; Marks, T. J.; Ratner, M. A. *J. Am. Chem. Soc.* **1998**, *120*, 11174−11181. (c) Kang, H.; Facchetti, A.; Zhu, P.; Jiang, H.; Yang, Y.; Cariati, E.; Righetto, S.; Ugo, R.; Zuccaccia, C.; Macchioni, A.; Stern, C. L.; Liu, Z.; Ho, S.-T.; Marks, T. J. *Angew. Chem., Int. Ed.* **2005**, *44*, 7922−7925. (d) Kang, H.; Facchetti, A.; Jiang, H.; Cariati, E.; Righetto, S.; Ugo, R.; Zuccaccia, C.; Macchioni, A.; Stern, C. L.; Liu, Z.; Ho, S.-T.; Brown, E. C.; Ratner, M. A.; Marks, T. J. *J. Am. Chem. Soc.* **2007**, *129*, 3267−3286.
(18) Rettig, W.; Bliss, B.; Dirnberger, K. *Chem. Phys. Lett.* **1999**, *305*, 8−14.
(19) (a) Jödicke, C. J.; Lüthi, H. P. *J. Am. Chem. Soc.* **2003**, *125*, 252−264. (b) Jödicke, C. J.; Lüthi, H. P. *J. Chem. Phys.* **2003**, *119*, 12852−12865.
(20) (a) Amatatsu, Y. *Theor. Chem. Acc.* **2000**, *103*, 445−450. (b) Amatatsu, Y. *Chem. Phys.* **2001**, *274*, 87−98. (c) Amatatsu, Y. *J. Phys. Chem. A* **2006**, *110*, 8736−8743.
(21) Gruen, H.; Görner, H. *Z. Naturforsch.* **1983**, *38a*, 928−936.
(22) (a) Safarzadeh-Amiri, A. *Chem. Phys. Lett.* **1986**, *125*, 272−278. (b) Rechthaler, K.; Köhler, G. *Chem. Phys. Lett.* **1996**, *250*, 152−158. (c) Eilers-König, N.; Kühne, T.; Schwarzer, D.; Vöhringer, P.; Schroeder, J. *Chem. Phys. Lett.* **1996**, *253*, 69−76. (d) Il'ichev, Y. V.; Kühnle, W.; Zachariasse, K. A. *Chem. Phys.* **1996**, *211*, 441−453. (e) Il'ichev, Y. V.; Zachariasse, K. A. *Ber. Bunsen-Ges. Phys. Chem.* **1997**, *101*, 625−635. (f) Lewis, F. D.; Weigel, W. *J. Phys. Chem. A* **2000**, *104*, 8146−8153. (g) Kovalenko, S. A.; Schanz, R.; Senyushkina, T. A.; Ernsting, N. P. *Phys. Chem. Chem. Phys.* **2002**, *4*, 703−707. (h) Arzhantsev, S.; Zachariasse, K. A.; Maroncelli, M. *J. Phys. Chem. A* **2006**, *110*, 3454−3470.
(23) Yang, J.-S.; Liau, K.-L.; Hwang, C.-Y.; Wang, C.-M. *J. Phys. Chem. A* **2006**, *110*, 8003−8010.
(24) Rappoport, D.; Furche, F. *J. Am. Chem. Soc.* **2004**, *126*, 1277−1284.
(25) (a) Minezawa, N.; Kato, S. *J. Phys. Chem. A* **2005**, *109*, 5445−5453. (b) Druzhinin, S. I.; Ernsting, N. P.; Kovalenko, S. A.; Lustres, L. P.; Senyushkina, T. A.; Zachariasse, K. A. *J. Phys. Chem. A* **2006**, *110*, 2955−2969.
(26) Fuss, W.; Pushpa, K. K.; Rettig, W.; Schmid, W. E.; Trushin, S. A. *Photochem. Photobiol. Sci.* **2002**, *1*, 255−262.
(27) Gómez, I.; Reguero, M.; Boggio-Pasqua, M.; Robb, M. A. *J. Am. Chem. Soc.* **2005**, *127*, 7119−7129.
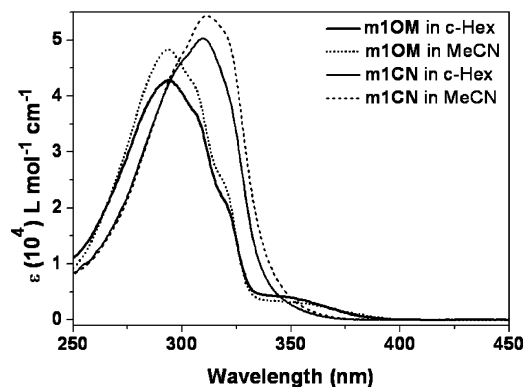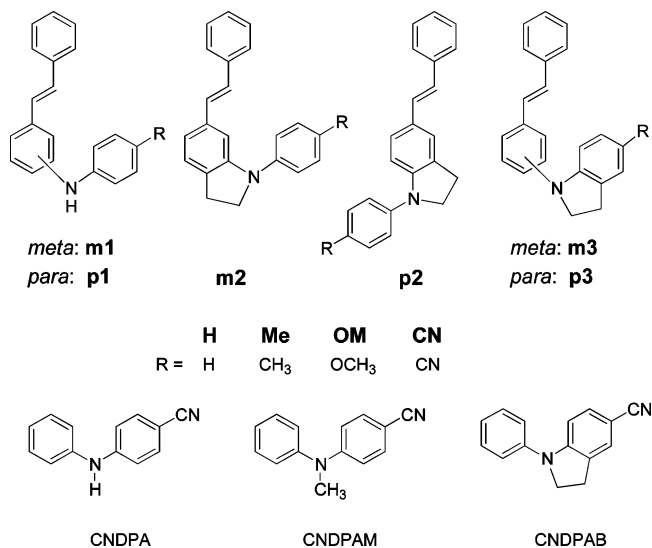
Figure 2. Electronic absorption spectra of **m1OM** and **m1CN** in cyclohexane (*c*-Hex) and acetonitrile (MeCN).

The photoisomerization competes with fluorescence in accounting for the deactivation of excited *trans*-stilbenes. Unlike the case of the D−A single-bond torsion, the structural effects on the double-bond torsion are well documented.[28−32] We have recently shown that the double-bond torsion does not couple with the single-bond torsion in *trans*-aminostilbenes, and thus, deactivation of the TICT state is mainly by heat.[23,32] Therefore, formation of a TICT state for *trans*-aminostilbenes can be readily detected based on their solvent-dependent fluorescence (Φ_f) and photoisomerization (Φ_{tc}) quantum yields, and there is no need to know if the TICT state is fluorescent or which bond is twisted.[23,32] With this advantage and the structural variability, *trans*-aminostilbenes are excellent candidates for gaining insights into the structural effects on the excited-state D−A single-bond torsional motions.

In this paper, we would like to address the meta vs para conjugation effect on TICT state formation through investigation of a series of *trans*-3-(*N*-arylamino)stilbenes (**m1**) and their ring-bridged derivatives (**m2** and **m3**) and through comparison with the previously reported para isomers (**p1**).[32] The results reported herein not only explicitly show that the degree of conjugation interactions in the ICT state plays an important role in TICT state formation but also provides the first experimental evidence for thermodynamically favorable but kinetically unfavorable D−A torsional motions. More specifically, unlike the TICT-forming **p1CN**, TICT state formation is negligible for **m1CN**, although both compounds possess a low-lying TICT state. This argument is in part based on the fact that the truncated molecule CNDPA undergoes efficient TICT formation in acetonitrile,[33] which is corroborated by the behavior of its *N*-methyl and ring-bridged compounds CNDPAM and CNDPAB. Another example

of conjugation-dependent TICT behavior is provided by the isomers **m1Me** and **p1Me**. Whereas **m1Me** undergoes TICT state formation in acetonitrile, aminostilbene **p1Me** is TICT free in spite of having a larger driving force for TICT formation. Implications of these results on the TICT dynamics of DCS and 3DMABN will also be addressed.

Results and Discussion

Electronic Spectra. The absorption spectra of **m1OM** and **m1CN** in cyclohexane and acetonitrile are shown in Figure 2. The spectra for **m1H** have been reported.[31] Both the spectra of **m1H** and **m1Me** resemble those of **m1OM**, where the most intense bands are located near 295 nm and there also exists a low-intensity broad shoulder near 340 nm, corresponding to $S_0 \rightarrow S_2$ and $S_0 \rightarrow S_1$ transitions, respectively. According to our previous studies on the "*m*-amino conjugation effect",[31] this can be attributed to band splitting as a result of configuration interactions (i.e., electronic coupling) between the meta-bridged subunits. Spectral deconvolution with Gaussian bands allows one to estimate the peak maxima (λ_{abs}) and oscillator strengths (*f*) for the $S_0 \rightarrow S_1$ transition. These data are presented in Table 1. In contrast, no distinct shoulder was observed for the spectra of **m1CN**, although there is a significant tailing in the red edge of the absorption band. The absorption maxima (310 nm) are red shifted with respect to that for **m1OM** (294 nm), but the red edges (∼375 nm) of the spectra are at shorter wavelength than those for **m1OM** (∼400 nm). Evidently, the band splitting is also present but weaker in **m1CN**. Since the electron-donating amino group plays an important role in determining the magnitude of electronic coupling,[6] the weaker band splitting in **m1CN** can be ascribed to the strong electron-withdrawing CN group that reduces the electron-donating ability of the anilino group. As a result, the 0,0 transitions derived from the intersection of normalized absorption and fluorescence spectra (vide infra) are at shorter wavelengths and the *f* values are lower for **m1CN** than for the other three **m1** derivatives (Table 1).

Figure 3 shows the fluorescence spectra of **m1Me**, **m1OM**, and **m1CN** in a variety of solvents. The corresponding spectra of **m1H** have been reported.[31] The fluorescence spectra of **m1** are structureless in both nonpolar and polar solvents, as observed for many other 3-aminostilbenes.[29] The lack of well-resolved vibrational bands even in nonpolar cyclohexane solvent might

(28) (a) Saltiel, J.; Charlton, J. L. *Rearrangements in Ground and Excited States*; de Mayo, P., Ed.; Academic Press: New York, 1980; Vol. 3, pp 25−89. (b) Saltiel, J.; Sun, Y.-P. *Photochromism, Molecules and Systems*; Dürr, H., Bouas-Laurent, H., Eds.; Elsevier: Amsterdam, 1990, pp 64−164. (c) Waldeck, D. H. *Chem. Rev.* **1991**, *91*, 415−436. (d) Meier, H. *Angew. Chem., Int. Ed. Engl.* **1992**, *31*, 1399−1420. (f) Görner, H.; Kuhn, H. J. *Adv. Photochem.* **1995**, *19*, 1−117.
(29) (a) Lewis, F. D.; Kalgutkar, R. S.; Yang, J.-S. *J. Am. Chem. Soc.* **1999**, *121*, 12045−12053. (b) Lewis, F. D.; Weigel, W. *J. Phys. Chem. A* **2000**, *104*, 8146−8153. (c) Lewis, F. D.; Weigel, W.; Zuo, X. *J. Phys. Chem. A* **2001**, *105*, 4691−4696.
(30) (a) Yang, J.-S.; Chiou, S.-Y.; Liau, K.-L. *J. Am. Chem. Soc.* **2002**, *124*, 2518−2527. (b) Yang, J.-S.; Wang, C.-M.; Hwang, C.-Y.; Liau, K.-L.; Chiou, S.-Y. *Photochem. Photobiol. Sci.* **2003**, *2*, 1225−1231.
(31) Yang, J.-S.; Liau, K.-L.; Tu, C.-W.; Hwang, C.-Y. *J. Phys. Chem. A* **2005**, *109*, 6450−6456.
(32) Yang, J.-S.; Liau, K.-L.; Wang, C.-M.; Hwang, C.-Y. *J. Am. Chem. Soc.* **2004**, *126*, 12325−12335.
(33) (a) Kapelle, S.; Rettig, W.; Lapouyade, R. *Chem. Phys. Lett.* **2001**, *348*, 416−424. (b) Kapelle, S.; Rettig, W.; Lapouyade, R. *Photochem. Photobiol. Sci.* **2002**, *1*, 492−499.

Table 1. Maxima of UV Absorption (λ_{abs}) and Fluorescence (λ_f), Fluorescence-Band Half-Width ($\Delta\nu_{1/2}$), 0,0 Transition ($\lambda_{0,0}$), Stokes Shifts ($\Delta\nu_{st}$), and Oscillator Strength (*f*) for the $S_0 \rightarrow S_1$ Band of **m1**−**m3**, **p1**, and CNDPAs in Cyclohexane (*c*-Hex) or Hexane (Hex) and Acetonitrile (MeCN)*a*

compd	solvent	λ_{abs} (nm)*b*	λ_f (nm)*c*	$\Delta\nu_{1/2}$ (cm^{-1})	$\lambda_{0,0}$ (nm)*d*	$\Delta\nu_{st}$ (cm^{-1})*e*	*f*^{f}
m1CN	*c*-Hex	310 (349)	397	4012	363	3464	0.02
	MeCN	311 (348)	434	4227	371	5694	0.03
p1CN^g	Hex	341	381 (399)	2712	370	3079	
	MeCN	352	425 [517]	8086	387	4880	
m1H	*c*-Hex	294 (335)	403	3716	371	5037	0.10
	MeCN	294 (336)	473	4316	395	8620	0.08
m1Me	*c*-Hex	294 (341)	411	3737	378	4995	0.07
	MeCN	293 (341)	497	4763	399	9205	0.08
p1Me^g	Hex	349	385 (402)	2808	374	2679	
	MeCN	354	457	3866	398	6367	
m1OM	*c*-Hex	294 (342)	417	3674	382	5259	0.08
	MeCN	293 (343)	>650				0.08
m2Me	*c*-Hex	301 (363)	(415) 436	3625	400	4612	0.12
	MeCN	302 (364)	500	3980	423	7473	0.14
m2OM	*c*-Hex	299 (364)	(422) 444	3495	405	4950	0.11
	MeCN	300 (366)	525	4179	433	8275	0.13
m3CN	*c*-Hex	310 (350)	399	3798	368	3509	0.03
	MeCN	326 (352)	479	4475	387	7532	0.03
CNDPA	*c*-Hex	302	363	3901	331	5564	
	MeCN	313	489	5146	361	11 499	
CNDPAM	*c*-Hex	297	383	3714	348	7560	
	MeCN	300	501	4665	364	13 373	
CNDPAB	*c*-Hex	324	356	2881	343	2774	
	MeCN	331	392	4249	356	4701	

a Fluorescence data are from corrected spectra. *b* The peak maxima of the long-wavelength shoulders are given in parentheses. *c* The vibronic shoulders are given in parentheses, and the second emission band is given in brackets. *d* The value of $\lambda_{0,0}$ was obtained from the intersection of normalized absorption and fluorescence spectra. *e* $\Delta\nu_{st} = \nu_{abs}$ ($S_0 \rightarrow S_1$) − ν_f. *f* $f = 4.3 \times 10^{-9} \int(\nu) \, d\nu$. *g* From ref 32.
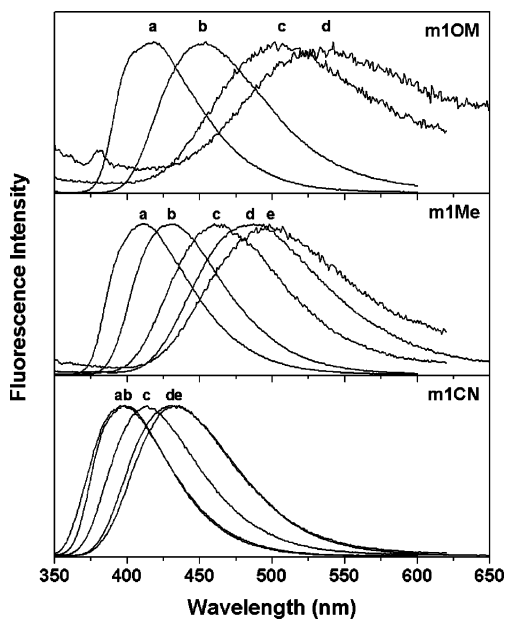

Figure 3. Normalized fluorescence spectra of **m1OM**, **m1Me**, and **m1CN** in (a) cyclohexane, (b) toluene, (c) dichloromethane, (d) acetone, and (e) acetonitrile.

be in part due to a less planar conformation about the stilbenyl−anilino C−N bond because the fluorescence spectrum for the ring-bridged derivatives **m2Me** and **m2OM** display vibrational bands in cyclohexane (Table 1 and Figure S4). Unlike the absorption spectra, the fluorescence maxima show a considerable red shift on going from cyclohexane to acetonitrile, indicating

Table 2. Ground- and Excited-State Dipole Moments for **m1**−**m3** and CNDPAs

compound	*a* (Å)*a*	m_f (cm^{-1})*b*	μ_g (D)*c*	μ_e (D)*d*
m1CN	4.90	7732	4.43	8.5 ± 0.5*e* (9.1^f)
m1H	4.76	11 524	0.89	11.5 ± 0.6 (10.8)
m1Me	4.84	12 901	1.00	12.6 ± 0.5 (11.8)
m1OM	4.93	16 443	0.73	14.3 ± 0.8 (13.6)
m2Me	4.98	8822	1.17	11.0 ± 0.5
m2OM	5.06	10 849	1.67	12.7 ± 0.5 (11.7)
m3CN	5.04	12 908	4.21	11.8 ± 0.7*e* (8.7)
CNDPA	4.25	20 788	4.55	15.1 ± 0.7
CNDPAM	4.35	18 995	5.12	15.3 ± 0.6
CNDPAB	4.44	8061	4.32	10.8 ± 0.6

a Onsager radius from eq 3 with $d = 1.0$ g/cm^3 for all cases. *b* Calculated based on eq 1. *c* Calculated by use of AM1. *d* Value in the parentheses is the dipole moment of the para isomer; data from ref 32. *e* Calculated with $-0.5\mu_g$. *f* Dipole moment of the PICT state of **p1CN**.

a strong ICT character for the S_1 state of **m1**. It should be noted that the spectra in polar solvents are relatively broader for **m1OM** and **m1Me** than **m1CN**. The fluorescence maxima (λ_f), the half-bandwidth ($\Delta\nu_{1/2}$), and the Stokes shift ($\Delta\nu_{st}$) are reported in Table 1.

To estimate the dipole moment of the fluorescing state (μ_e), the slopes (m_f) of the solvatofluorochromic plots of the energies of the fluorescence maxima against the solvent parameter Δf (Figures S1−S2) were obtained according to eq 1[34]

$$\nu_f = -[(1/4\pi\epsilon_0)(2/hca^3)][\mu_e(\mu_e - \mu_g)]]\cdot\Delta f + \text{constant} \quad (1)$$

where

$$\Delta f = (\epsilon - 1)/(2\epsilon + 1) - 0.5(n^2 - 1)/(2n^2 + 1) \quad (2)$$

and

$$a = (3M/4N\pi d)^{1/3} \quad (3)$$

where ν_f is the fluorescence maximum, μ_g is the ground-state dipole moment, a is the solvent cavity (Onsager) radius, which was derived from Avogadro's number (*N*), molecular weight (M), and density (*d*), and ϵ, ϵ_0, and *n* are the solvent dielectric constant, vacuum permittivity, and solvent refractive index, respectively. The value of μ_g was calculated using the MOPAC-AM1 algorithm.[35] The calculated values of a, m_f, μ_e, and μ_g for **m1** are summarized in Table 2. The relative values of m_f and thus μ_e are **m1OM** > **m1Me** > **m1H** > **m1CN**, as expected based on the relative electron-donating ability of the anilino groups. It should be noted that the ground- and excited-state dipoles in **m1CN** are in different directions, which are amino N → benzonitrilo and amino N → stilbenyl, respectively. Assuming that the angle between the ground- and excited-state dipoles of **m1CN** is ca. 120°, the calculated ground-state dipole would have a component vector of $0.5\mu_g$ (i.e., cos(120°) μ_g) in a direction opposite to the excited-state dipole. Accordingly, a negative value of $-0.5\mu_g$ was adopted for eq 1 in calculating μ_e for **m1CN**, resembling the case of **p1CN**.[32]

Upon ring bridging for **m1** (i.e., derivatives **m2OM**, **m2Me**, and **m3CN**), noticeable changes in the electronic spectra are observed. For **m2OM** and **m2Me**, both the first ($S_0 \rightarrow S_1$) and the second ($S_0 \rightarrow S_2$) absorption maxima shift toward the red,

(34) Baumann, W.; Bischof, H.; Fröhling, J.-C.; Brittinger, C.; Rettig, W.; Rotkiewicz, K. *J. Photochem. Photobiol. A: Chem.* **1992**, *64*, 49−72.
(35) Dewar, M. J. S.; Zoebisch, E. G.; Healy, E. F.; Stewart, J. J. P. *J. Am. Chem. Soc.* **1985**, *107*, 3902−3909.
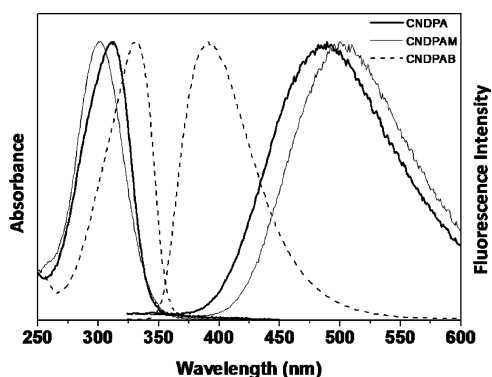
Figure 4. Normalized absorption and fluorescence spectra of CNDPA, CNDPAM, and CNDPAB in acetonitrile.

which is as expected due to the additional *N*-ethylene group (Table 1, Figure S3). We also note that the relative intensity for the first vs the second band and the magnitude of band splitting in **m2OM** and **m2Me** are slightly larger (~3% more for the relative intensity and ~1000 cm^{-1} more between the two bands) than those in the parent **m1OM** and **m1Me**, respectively. Evidently, increasing the electron-donating ability and planarity of the amino group enhances the electronic coupling through the *m*-Ph bridge. Furthermore, ring bridging leads to more structured fluorescence spectra in cyclohexane (Figure S4), indicating that the structureless fluorescence spectra of *trans*-3-aminostilbenes[31,36] in nonpolar solvents is associated with the degree of D–A coplanarity in the fluorescing state. Moreover, the fluorescence spectra in polar solvents become sharper for the ring-bridged derivatives. Because of the different ring-bridging position, the resulting changes in both absorption and fluorescence spectra on going from **m1CN** to **m3CN** appear to be smaller. In addition, it is interesting to note that the difference in the ring-bridging position results in a different effect on the excited-state dipole moment, where it is increased on going from **m1CN** to **m3CN** but decreased on going from **m1Me** and **m1OM** to **m2Me** and **m2OM** (Table 2). The smaller excited-state dipole moment for **m2** vs **m1** appears to be in conflict with the stronger electronic coupling and donor strength. Evidently, the less planar structure in the fluorescing state of **m1** promotes a larger degree of charge separation and thus a larger dipole moment.

Compound CNDPA is a truncated molecule of **m1CN** and **p1CN** by removing the styryl group. The fluorescence spectrum of CNDPA in acetonitrile has been reported,[33] but more detailed spectroscopic data were not presented. As such, we carried out studies on CNDPA as well as its *N*-methyl and ring-bridged derivatives CNDPAM and CNDPAB. Figure 4 shows the normalized absorption and fluorescence spectra of CNDPA, CNDPAM, and CNDPAB in acetonitrile, and more spectroscopic data are shown in Table 1. It is interesting to note that the absorption maximum is CNDPAB > CNDPA > CNDPAM in both cyclohexane and acetonitrile, but their fluorescence maxima show an opposite order in acetonitrile (i.e., CNDPAM > CNDPA > CNDPAB) and an order of CNDPAB > CNDPAM > CNDPA in cyclohexane. The unexpected blue shift of the absorption maximum for CNDPAM vs CNDPA clearly shows that the absorption maximum is very sensitive to

(36) Karabunarliev, S.; Baumgarten, M.; Tyutyulkov, N.; Müllen, K. *J. Phys. Chem.* **1994**, *98*, 11892–11901.

Table 3. Quantum Yields for Fluorescence (Φ_f) and Photoisomerization (Φ_{tc}), Fluorescence Decay Times (τ_f), and Rate Constants for Fluorescence Decay (k_f) and Nonradiative Decay (k_{nr}) for **m1**–**m3**, **p1**, and CNDPAs in Solution

compd	solvent	Φ_f	$\Phi_{tc}{}^a$	τ_f/ns^b	k_f (10^7 s^{-1})	k_{nr} (10^7 s^{-1})
m1CN	*c*-Hex	0.52	0.23	10.1	5.1	4.7
	THF	0.49				
	CH$_2$Cl$_2$	0.42	0.27	8.6	4.9	6.8
	MeCN	0.37	0.32	14.0	2.6	4.5
p1CN^c	Hex	0.75	0.16	1.30	58	19
	MeCN	0.015	0.04^d	0.84	1.8	117
m1H^e	*c*-Hex	0.57	0.23^d	14.8^d	3.8^d	2.9^d
	THF	0.32				
	CH$_2$Cl$_2$	0.29	0.38^c	9.2^d	3.1^d	7.7^d
	MeCN	0.17	0.42^d	10.0^d	1.7^d	8.3^d
m1Me	*c*-Hex	0.56	0.22	13.4	4.2	3.3
	THF	0.22				
	CH$_2$Cl$_2$	0.18	0.41	7.7	2.3	10.7
	MeCN	0.08	0.25	6.1	1.3	15.0
p1Me^e	Hex	0.53		0.96	55	49
	MeCN	0.41	0.27^d	1.75	23	34
m1OM	*c*-Hex	0.48	0.25	13.4	3.6	3.9
	THF	0.07	0.29	5.0	1.4	18.6
	CH$_2$Cl$_2$	0.05	0.20	3.6	1.4	26.1
	MeCN	<0.003	0.04			
m2Me	*c*-Hex	0.65	0.15	8.9	7.3	3.9
	CH$_2$Cl$_2$	0.31		6.5	4.8	10.6
	MeCN	0.47	0.25	14.3	3.3	3.7
m2OM	*c*-Hex	0.73	0.18	10.3	7.1	2.6
	CH$_2$Cl$_2$	0.35	0.31	10.1	3.5	6.5
	MeCN	0.37		14.1	2.6	4.5
m3CN	*c*-Hex	0.39	0.27	11.3	3.5	5.4
	CH$_2$Cl$_2$	0.24		10.5	2.3	7.3
	MeCN	0.14	0.40	9.8	1.4	8.8
CNDPA	*c*-Hex	0.31		2.8	11.1	24.6
	MeCN	0.14		6.8	2.1	12.6
CNDPAM	*c*-Hex	0.34		4.3	7.9	15.3
	MeCN	0.14		9.9	1.4	8.7
CNDPAB	*c*-Hex	0.69		2.3	30.0	13.5
	MeCN	0.86		2.9	29.7	4.8

^{a} Containing 10% THF when determined in cyclohexane and acetonitrile by reason of solubility. ^{b} The value of τ_f was determined with excitation and emission around the spectral maxima, unless otherwise noted. ^{c} Data from ref 32. ^{d} Data from this work. ^{e} Data from ref 31.

the planarity of the molecule. In other words, the additional *N*-methyl group in CNDPAM increases the donor strength but concomitantly imposes larger steric demand that reduces the coplanarity of the two phenyl rings. The significantly red-shifted fluorescence spectrum for CNDPA vs CNDPAB in acetonitrile but not in cyclohexane indicates that the nature of the fluorescing state of CNDPA is different in these two solvents (i.e., TICT vs PICT, vide infra). It should also be noted that the dipole moment for the fluorescing state is much larger for CNDPA and CNDPAM than for CNDPAB (Table 2).

Quantum Yields and Lifetimes. Fluorescence quantum yields for **m1** were determined in cyclohexane, THF, dichloromethane, and acetonitrile. As shown in Table 3, all four species are strongly fluorescent in cyclohexane, but the values of Φ_f decrease in more polar solvents. Compounds **m1OM** and **m1CN** display the most and the least sensitive dependence of Φ_f on the solvent polarity, respectively (i.e., **m1OM** > **m1Me** > **m1H** > **m1CN**).

Quantum yields for trans → cis photoisomerization for **m1** in selected solvents are also reported in Table 3. It is well known that photoisomerization of *trans*-stilbenes can occur via the singlet (^{1}t*) and triplet (^{3}t*) state.[28] Either decay pathway involves an intermediate perpendicular state (^{1}p* or ^{3}p*) located at the conical intersection from which a state jump can lead to

the trans or cis isomer with a similar probability (i.e., ~50%). Whereas the process of $^1t^* \rightarrow {}^1p^*$ involves a thermal barrier, it is essentially barrierless for the process of $^3t^* \rightarrow {}^3p^*$. The latter in turn suggests that nearly all the intersystem crossing processes $^1t^* \rightarrow {}^3t^*$ would lead to the double-bond torsion. As a result, the doubled amount of the determined trans → cis photoisomerization quantum yield (Φ_{tc}) would approximately correspond to the sum of the quantum yields for singlet-state double-bond torsion (Φ_d) and $S_1 \rightarrow T_1$ intersystem crossing (Φ_{isc}): namely, $2\Phi_{tc} = \Phi_d + \Phi_{isc}$. Previous studies have shown that *trans*-4-aminostilbenes mainly adopt the singlet mechanism (i.e., $2\Phi_{tc} \approx \Phi_d$) but the triplet mechanism predominates in *trans*-3-aminostilbenes (i.e., $2\Phi_{tc} \approx \Phi_{isc}$) due to a large singlet-state torsional barrier.[29-32] Disregarding the exact photoisomerization mechanism, the value of $\Phi_f + 2\Phi_{tc}$ allows one to determine if new decay channels other than fluorescence and photoisomerization are present for $^1t^*$. As shown in Table 3, except for **m1Me** in acetonitrile and **m1OM** in THF or more polar solvents, the value of $\Phi_f + 2\Phi_{tc}$ is within the experimental error of 1.0 for **m1**, indicating that new decay pathways are negligible for the latter cases but should be taken into account for the former cases.

The values of Φ_f and Φ_{tc} for the ring-bridged aminostilbenes **m2OM**, **m2Me**, and **m3CN** are also reported in Table 3. Unlike **m1OM** and **m1Me** that possess a value of $\Phi_f + 2\Phi_{tc}$ much less than 1.0 in polar solvents, all three ring-bridged compounds conform to $\Phi_f + 2\Phi_{tc} \approx 1.0$ in both nonpolar and polar solvents.

The room-temperature fluorescence lifetimes (τ_f) determined with excitation and emission wavelengths around the spectral maxima for **m1**−**m3** in selected solvents are provided in Table 3. All the decays can be well fit by single-exponential functions, although more than one planar conformer is expected for all cases. Table 3 also shows the rate constants for fluorescence ($k_f = \Phi_f \tau_f^{-1}$) and the overall nonradiative deactivation processes ($k_{nr} = (1 - \Phi_f)/\tau_f^{-1}$). Both features of long decay times (>8 ns) in cyclohexane and lower k_f values in more polar solvents for **m1**−**m3** resemble the other *trans*-3-aminostilbenes.[29,31] However, upon monitoring at the red edge of the fluorescence spectra, dual exponential decays were observed for **m1Me** and **m1OM** in polar solvents such as dichloromethane and acetonitrile (Table S1). For example, the fluorescence maximum of **m1Me** in acetonitrile is at 497 nm, and a single decay time of 6.1 ns was obtained at 500, 525, and 550 nm. However, at 575 nm, biexponential fitting was required and the second decay time is a shorter lived component (0.05 ns) with a preexponential of ~0.2. Since the decay time is near the time resolution of our instrument (0.1 ns), it should be viewed as approximate. Likewise, a shorter lived component (~0.1 ns) was detected for **m1OM** in dichloromethane upon monitoring at longer emission wavelength (>575 nm). This shorter-lived component is of extremely weak fluorescence since it contributes less than 2% of the fluorescence even at the fluorescence tail of the longer lived component. The longer and shorter lived components could be attributed to the PICT and TICT states, respectively (vide intra).

Table 3 also shows the values of Φ_f and τ_f for CNDPA, CNDPAM, and CNDPAB in cyclohexane and acetonitrile. Both CNDPA and CNDPAM possess a larger Φ_f value in cyclohexane vs acetonitrile, but the opposite is true for CNDPAB. In addition, the value of τ_f is much larger in acetonitrile vs
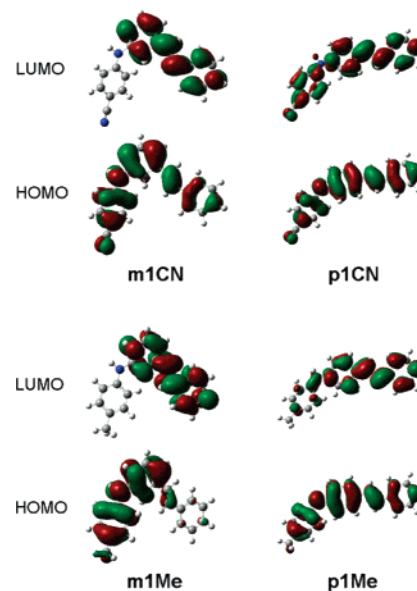

Figure 5. Frontier molecular orbital plots (B3LYP/6-31G(d,p)) of optimized structures of **m1CN**, **p1CN**, **m1Me**, and **p1Me**.

cyclohexane for CNDPA and CNDPAM but it is similar for CNDPAB. As a result, the k_f value is reduced by more than 5-fold for the former two species on going from cyclohexane to acetonitrile, but there is no change for CNDPAB. In conjunction with the fluorescence spectra (vide supra), our results support the previous TICT argument for CNDPA.[33] In other words, the observed fluorescence of CNDPA and CND-PAM in acetonitrile is almost entirely from their TICT state, which results from the twisting of the benzonitrilo−dimethylamino C−N bond, but the ICT state for them in cyclohexane should be planar (i.e., PICT), as is the case of the ring-bridged CNDPAB.

Conjugation Interactions in m1 vs p1. The spectroscopic data, excited-state dipole moments, and quantum yields for fluorescence and trans → cis isomerization for **p1**−**p3** have previously been reported.[32] To address the relative conjugation (charge-delocalization) interactions in **m1** vs **p1**, some of these data along with a couple of new data for **p1**, particularly **p1CN** and **p1Me**, are shown in Tables 1−3. In addition, the DFT (B3LYP level of theory,[37] 6-31G(d,p) basis set)-derived frontier molecular orbitals (FMOs) of **m1CN**, **p1CN**, **m1Me**, and **p1Me** are shown in Figure 5.

As reflected by the more localized absorption bands (~295 nm) vs the single-intense long-wavelength absorption band of charge-transfer character for **m1** vs **p1**, the ground-state conjugation interaction is as expected much weaker in the meta isomers. However, the presence of a low-intensity shoulder at longer wavelengths for **m1** indicates the presence of electronic coupling between the *m*-Ph-bridged subunits. Such an electronic coupling increases with increasing electron-donating ability of the anilino group (vide supra). In the excited state, the comparable dipole moments for **m1** and **p1** (Table 2) suggest that the charge-separated ICT process in the meta isomers is as efficient as that in the para isomers. However, the significantly longer fluorescence lifetimes and lower fluorescence rate constants for **m1** vs **p1** indicate a much slower charge-

(37) (a) Lee, C.; Yang, W.; Parr, R. G. *Phys. Rev. B* **1988**, *37*, 785−789. (b) Becke, A. D. *J. Chem. Phys.* **1993**, *98*, 5648−5652.

recombination process. This behavior resembles the larger D−A systems recently reported by Thompson et al.[7] and imposes an important effect on the molecular bonding character and thus the D−A torsional kinetics (vide infra). A weaker conjugation interaction for **m1** vs **p1** is also reflected by their FMOs, where the HOMO and LUMO of both **p1CN** and **p1Me** are delocalized, but the LUMOs of **m1CN** and **m1Me** are localized at the stilbene moiety, and their HOMOs are slightly localized at the diarylamino group.

Propensity of TICT Formation. We recently reported a simple guideline based on the values of Φ_f and Φ_{tc} for judging whether a TICT state is actively invoked in the excited decay of aminostilbenes.[23,32] To claim an important TICT state formation, two phenomena should be observed: (1) the value of Φ_f should be significantly smaller in polar vs nonpolar solvents, since the propensity of TICT state formation is larger in more polar solvents and the fluorescence quantum yield for TICT states is much lower than the precursor PICT state; (2) fluorescence and trans−cis photoisomerization cannot account for all the decay processes (i.e., $\Phi_f + 2\Phi_{tc} \ll 1.0$) because the process of photoisomerization is essentially decoupled with the TICT state deactivating processes. For example, **p1CN** has been shown to form a DMABN-like TICT state by twisting the benzonitrilo group in solvents more polar than THF.[32] The Φ_f value decreases by as much as 50 fold on going from hexane (0.75) to acetonitrile (0.015). In addition, the value of $\Phi_f + 2\Phi_{tc}$ for **p1CN** in hexane is 1.07 but only 0.095 in acetonitrile (Table 3). More evidence for TICT state formation of **p1CN** includes (a) the observation of PICT−TICT dual fluorescence in acetonitrile, (b) a significant reduction in the fluorescence rate constant (k_f) on going from hexane (5.8×10^8 s^{-1}) to acetonitrile (2.0×10^7 s^{-1}), (c) the dual fluorescence disappears and normal deactivating mode for *trans*-stilbenes (i.e., $\Phi_f + 2\Phi_{tc} \approx 1.0$) recovered when the torsional motion is inhibited through constrained ring bridging between the D and A groups (i.e., **p3CN**), and (d) the fluorescence intensity increases upon raising the temperature.[32] However, it should be noted that observation of a steady-state dual fluorescence (i.e., item a) is not a requirement for claiming formation of a TICT state because the TICT fluorescence could be extremely weak (vide infra). The evidence in item c not only confirms TICT state formation but also specifies the bond that is responsible for the torsional motion.

On the basis of the above guidelines we can readily conclude that TICT formation is negligible for **m1CN** in both cyclohexane ($\Phi_f = 0.52$ and $\Phi_f + 2\Phi_{tc} = 0.98$) and acetonitrile ($\Phi_f = 0.37$, $\Phi_f + 2\Phi_{tc} = 1.01$) (Table 3). This conclusion is corroborated by comparing with the TICT-forming **p1CN** and CNDPA and the TICT-inhibited ring-bridged model compounds **m3CN**, **p3CN**, and CNDPAB. For example, compared to **m1CN**, the smaller π-system CNDPA displays a fluorescence maximum at longer wavelength in acetonitrile (489 vs 434 nm) but at shorter wavelength in cyclohexane (363 vs 397 nm) (Table 1). In addition, the excited-state dipole moment is significantly larger for CNDPA (15.1 D) vs **m1CN** (8.5 D) (Table 2). For comparison, the dipole moments for the PICT and TICT state of **p1CN** are 9.1 and 16.4 D, respectively.[32] Moreover, unlike the dramatic differences in fluorescence properties between **p1CN** and **p3CN** and between CNDPA and CNDPAB in acetonitrile, the corresponding difference between **m1CN** and
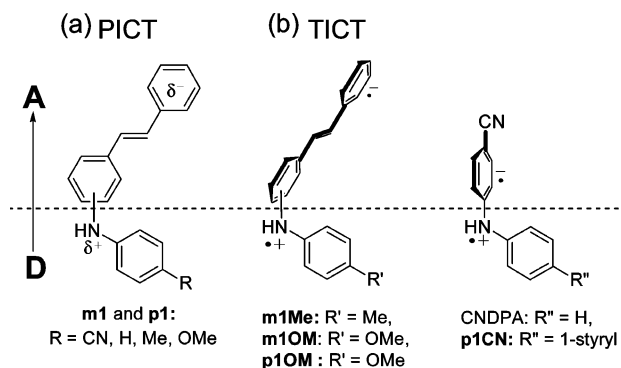

Figure 6. Schematic summary of the charge-transfer behavior of the PICT and TICT states of **m1** and **p1** and the TICT states of CNDPA in acetonitrile.

m3CN is rather small, which can be simply attributed to the minor substituent effect.

In contrast to the different ICT behavior between the isomers **m1CN** and **p1CN**, TICT state formation for **m1OM** is as efficient as that for **p1OM**.[32] This is manifested by the facts that the value of $\Phi_f + 2\Phi_{tc}$ substantially deviates from 1.0 in acetonitrile (~0.08) but not in cyclohexane (0.98) and the Φ_f value is significantly reduced on going from cyclohexane to acetonitrile (Table 3). Formation of a TICT state also accounts for the short-lived component in the decays of fluorescence upon detecting at the red edge of spectra (Table S1). The short lifetime (0.1 ns) for the TICT state indicates the presence of efficient nonradiative decay channels. On the basis of the behavior of $\Phi_f + 2\Phi_{tc} \approx 1.0$ and high Φ_f values for the ring-bridged derivative **m2OM** in both acetonitrile and dichloromethane (Table 3), torsion of the stilbenyl−anilino C−N bond in **m1OM** should be responsible for the TICT-forming process, as is the case of **p1OM**. The absence of well-resolved dual fluorescence for **m1OM** (Figure 3) in polar solvents also resembles the case of **p1OM** and can be attributed to the weak fluorescence of the TICT states.

A value of $\Phi_f + 2\Phi_{tc} = 0.58$ for **m1Me** in acetonitrile also suggests the participation of a TICT state in the excited decay. As indicated by the absence of steady-state dual fluorescence and the short TICT lifetime (0.05 ns), the nonradiative decay processes for the TICT state should be very efficient. The TICT state also results from the twisting of the stilbenyl−anilino C−N bond, as evidenced by the ring-bridged derivative **m2Me**. However, the efficiency of TICT formation is much lower for **m1Me** vs **m1OM** and becomes negligible in less polar solvents such as dichloromethane. This can be attributed to the weaker 4-methylanilino vs 4-methoxyanilino donor group. Nonetheless, formation of a TICT state for **m1Me** in acetonitrile is still in marked contrast to the para isomer **p1Me**, which is TICT free under the same condition.

Since the anilino donor in **m1H** is even weaker than the 4-methylanilino group in **m1Me** it is not unexpected to conclude that **m1H** is TICT free in both dichloromethane and acetonitrile on the basis of $\Phi_f + 2\Phi_{tc} \approx 1.0$ in all investigated solvents (Table 3). The para isomer **p1H** was also shown to be free of TICT state formation under the same condition. A summary of the ICT behavior of both **m1** and **p1** in acetonitrile is depicted in Figure 6.

Energy Diagram. The distinct TICT-forming propensity in **m1CN** vs **p1CN** and in **m1Me** vs **p1Me** explicitly shows that the D−A torsional motion depends not only on the relative
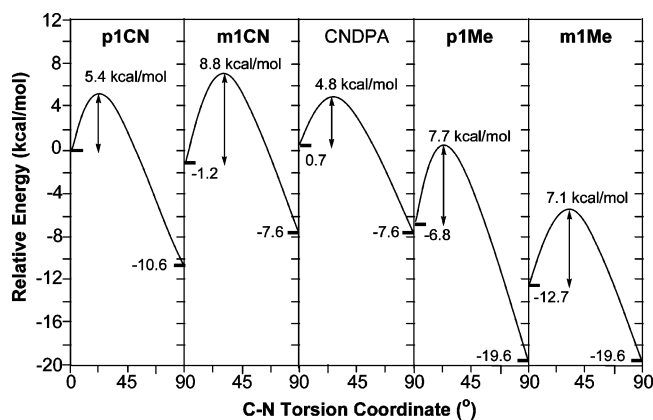
Figure 7. Potential-energy diagram for PICT → TICT through C−N bond torsion for **p1CN**, **m1CN**, CNDPA, **p1Me**, and **m1Me** in acetonitrile. Energies are relative to PICT of **p1CN**. Torsional barriers are derived from the Arrhenius equation at a preexponential factor of 10^{13}.

strength of the D and A groups but also on the structural nature of the D−A constitution. To elucidate the origin of the meta vs para effects on the torsional motion reaction in aminostilbenes **1CN** and **1Me** one needs to compare the relative energies of the related states for both isomers: namely, to construct the state energy diagrams. However, to obtain the real quantitative energy diagram of different states for a specific compound is essentially impossible regarding the facts that (1) the exact structures of the PICT and TICT states are unknown and (2) as reflected by the broad fluorescence spectra there should exist a broad distribution of substrate/solvent structures and thus the state energies in each state. Nonetheless, under reasonable assumptions it might be possible to construct a relative and qualitative energy diagram for the purpose of comparison of the meta and para isomers. Since the differences between **p1Me** and **m1Me** are more significant in acetonitrile and acetonitrile has been the most common solvent for discussing the TICT behavior of arylamines, the following analysis and discussion will based on the data in acetonitrile. First, we assume that the 0,0 transition energy ($\lambda_{0,0}$) corresponds to the transition from the optimized ground state to the Franck−Condon (FC) excited state. In addition, the PICT and TICT fluorescence maxima ($\lambda_{f,PICT}$ and $\lambda_{f,TICT}$) were assumed to correspond to the averaged transition energies from the PICT and TICT states to their FC ground states, respectively. When the TICT fluorescence band is not resolved from the PICT band (e.g., **p1Me** and **p1OM**) or when the TICT state is not even formed (e.g., **m1CN**), other treatments would be made (see Supporting Information). Second, the relative energies of the optimized ground state and the FC ground states of PICT and TICT were evaluated by DFT calculations (Figure S5).[37] The FC ground states of TICT were assumed to have a perpendicular geometry between the D (anilino or stilbenylamino group) and the A (benzonitrilo or stilbenyl group), where the D and the A groups are in a planar form. For the FC ground states of PICT it was assumed that the amino nitrogen is coplanar with the stilbenyl group and the rest part of the structure was optimized.

While the detailed energy diagrams about the optimized, PICT, and TICT states in S_0 and S_1 for CNDPA and the meta and para isomers of **1CN** and **1Me** in acetonitrile are provided as Supporting Information (Figures S6 and S7), Figure 7 shows the relative energies of their PICT and TICT states. It is interesting to note that the TICT states are at lower energies

than the corresponding PICT states in all five cases, but only three of them (i.e., **p1CN**, CNDPA, and **m1CN**) display significant TICT state formation. In particular, the driving force for the TICT state formation for **m1CN** is similar to that for CNDPA (>6.4 vs 8.3 kcal/mol), but the outcome is entirely different: namely, one is negligible but the other is almost complete. Furthermore, **p1Me** has a larger driving force for TICT state formation than **m1Me**, but the propensity of TICT state formation is in the opposite trend. Evidently, the torsional motion toward the TICT state for **m1CN** and **p1Me** must be too slow to compete with fluorescence and the nonradiative isomerization process. Since the rate constants for fluorescence and isomerization for **m1CN** in acetonitrile are 2.6×10^7 and 4.5×10^7 s^{-1}, respectively (Table 3), the rate constant for the single-bond torsion (k_{TICT}) would be at least 1 order of magnitude lower than that for fluorescence (i.e., $k_{TICT} < 3 \times 10^6$ s^{-1}). Assuming that the preexponential factor for the single-bond torsion is in the order of 10^{13} at room temperature (23 °C), the resulting torsional barrier would be 8.8 kcal/mol. Likewise, the rate constants for fluorescence and isomerization for **p1Me** in acetonitrile are 2.3×10^8 and 3.4×10^8 s^{-1}, respectively, the rate constant for the torsional motion should be at least 1 order of magnitude lower (i.e., $k_{TICT} < 2 \times 10^7$ s^{-1}). With the assumption of a preexponential factor of 10^{13} for the single-bond torsion, the resulting torsional barrier would be 7.7 kcal/mol. For comparison, the k_{TICT} values for **p1CN** and **m1Me** are $\sim 1 \times 10^9$ s^{-1} ($\Phi_{TICT} = 1 - \Phi_f - 2\Phi_{tc} \approx 0.9$) and $\sim 6 \times 10^7$ s^{-1} ($\Phi_{TICT} = 1 - \Phi_f - 2\Phi_{tc} \approx 0.42$), respectively, corresponding to a barrier of ~ 5.4 and ~ 7.1 kcal/mol at a preexponential factor of 10^{13}. In the case of CNDPA, the k_{TICT} value should be at least 1 order of magnitude larger than the k_f value of its PICT state in order to account for the absence of PICT fluorescence (Figure 4). On the basis of the k_f value for CNDPAB in acetonitrile (Table 3), a value of $k_{TICT} > 3 \times 10^9$ s^{-1} and thus a torsional barrier of <4.8 kcal/mol is predicted for CNDPA. These relative torsional barriers are also shown in Figure 7. It is interesting to note that the difference in the torsional barrier between **m1Me** and **p1Me** (**m1Me** < **p1Me**) is much smaller than that between **m1CN** and **p1CN** (**m1CN** ≫ **p1CN**).

Origin of the Torsional Barrier. Although kinetic controlled reactions are well known in thermal organic reactions, the conclusion of a kinetic but not thermodynamic inhibition of TICT state formation (i.e., **m1CN** and **p1Me**) is unprecedented and deserves further discussion. As presented in the following, the differences in the propensity of TICT formation for the meta vs para isomers of **1CN** and **1Me** can be both attributed to their differences in charge-delocalization interactions in the precursor PICT states, which are weaker for the meta isomers.

To understand the negligible TICT formation for **m1CN** it should be reminded that there is an inherent difference in the charge-transfer direction between the PICT and TICT states of **1CN** (Figure 6). In analogy to the cases of **p1CN** and CNDPA, the TICT state for **m1CN** should also result from the twisting of the stilbenylamino (D)−benznitrilo (A) C−N bond. This is in marked contrast to the PICT state, where charge transfer is from the anilino (D) to the stilbenyl (A) group. Thus, to initiate the single-bond torsional motion from the PICT state, the charge must be translocated from one end of the molecule to the other in order to induce changes in both the nuclear coordinate and
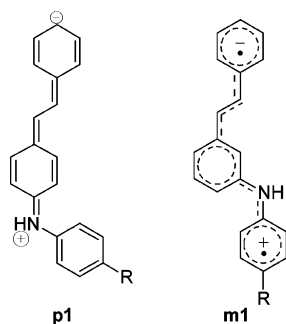
Figure 8. Schematic representation of the resonance-induced quinoidal character of **p1** and the radical ion-pair character of **m1** in the PICT states.

the reorientation of the solvent dipoles. While charge delocalization is expected to be feasible in **p1CN** due to the *p*-Ph bridge, it is blocked to a significant extent by the *m*-Ph bridge in **m1CN**, as indicated by the slow charge-recombination process and the localized LUMO (Figure 5). In conjunction with the smaller thermodynamic driving force for **m1CN** vs **p1CN**, the barrier for the torsion toward TICT is expected to be much higher for **m1CN** vs **p1CN**, which accounts for their distinct propensity for TICT state formation.

The situation is different in **p1Me** and **m1Me** because the charge-transfer direction for their PICT and TICT states is the same and, unlike the case of **p1CN**, the TICT state results from the twisting of the stilbenyl (A)−anilino (D) C−N bond (Figure 6b). Since the single-bond torsion has the same starting point as the double-bond torsion in **p1Me**, the much more efficient double- vs single-bond torsion in **p1Me** explicitly indicates that its PICT state possesses a strong quinoidal character. This is consistent with the resonance-derived picture for the PICT state (Figure 8), which have been successfully applied for understanding the efficiency of trans−cis photoisomerization of *trans*-4-aminostilbenes.[29,30] The large double-bond character for the stilbenyl−anilino C−N bond would lead to a large torsional barrier. Since the resonance is blocked by the *m*-Ph bridge in **m1Me**, the PICT state might be better described as an electron transfer from the anilino (D) to the stilbenyl (A) group (i.e., a radical ion-pair character) (Figure 8). This in turn suggests a less double-bond character for the stilbenyl−anilino C−N bond and thus a lower barrier for its torsion. Indeed, this picture is consistent with the argument of less planar PICT states for **m1** vs **p1** on the basis of the less structured fluorescence spectra in nonpolar solvents. Nonetheless, the discussion in the Energy Diagram section has suggested that the D−A torsional barrier for **p1Me** vs **m1Me** is not necessarily much higher. This might be in part attributed to the larger thermodynamic driving force for **p1Me**, which would lower the barrier to some extent. In addition to the torsional barrier, another important factor that accounts for the absence of TICT formation for **p1Me** is its large fluorescence and photoisomerization decay rates (Table 3), which further reduces the competition of the TICT-forming process.

The origin of negligible TICT formation for **p1Me** might also be responsible for the case of DCS, which shows no TICT behavior but appears to have a low-lying TICT state resulting from the twisting of the styryl−anilino C_{st}−C_{an} bond.[20] In other words, the PICT state of DCS possesses a quinoidal structure with the C_{st}−C_{an} bond of a large double-bond character, resembling the case of **p1Me** (Figure 8). Indeed, the quinoidal

picture for DCS is consistent with its large rates of isomerization and fluorescence ($2.5-16.7 \times 10^8$ s^{-1}) in acetonitrile.[21]

Our results could also provide insights into the distinct TICT-forming propensity between 3DMABN and DMABN. Both the experimental (e.g., solvatofluorochromism)[18] and theoretical studies[19] have indicated that the LE state of 3DMABN possesses a larger charge-transfer character (i.e., mixed ^1L_a/^1L_b character) than that of DMABN (^1L_b). This in turns might suggest that the LE state of 3DMABN is of some quinoidal character, and thus, the benznitrilo−dimethylamino C−N bond possesses some double-bond character. This is different from the case of DMABN, the LE state of which has recently been suggested to be of antiquinoidality.[24] Furthermore, like the case of **m1Me** vs **p1Me**, the LE state of 3DMABN is lower in energy by ∼10 kcal/mol than that for DMABN,[14] corresponding to a smaller thermodynamic driving force toward the TICT state.

While all the above discussion about the mechanism of TICT formation conforms to the adiabatic precursor (PICT)−successor (TICT) model, a nonadiabatic reaction mechanism has recently been shown to play an important role in accounting for the TICT formation in DMABN.[26,27] The latter mechanism suggests that the TICT state is directly formed from the FC structure on S$_2$ through a conical intersection, corresponding to a nearly barrierless TICT-forming pathway. In this context, the absence of TICT formation for 3DMABN might suggest that the nonadiabatic route is either rather inefficient or significantly distorted toward the LE state because of the lower LE state and the higher torsional barrier toward the TICT state. Such a nonadiabatic route appears to be unimportant for *trans*-aminostilbenes in view of the different electronic structures from the DMABN systems: namely, the polar PICT state is the S$_1$ state rather than the S$_2$ state in aminostilbenes.

Concluding Remarks

The most important finding in this work is that the presence of a low-lying TICT state for a D−A system is insufficient to argue for its formation because the rate of the torsional motion could be too slow to compete with the other deactivation channels. The evidence relies on the distinct TICT-forming propensity between the meta and the para isomers of *trans*-aminostilbenes **1CN** and **1Me**. According to their energy diagrams, the PICT → TICT process is exothermic for all four cases, and the thermodynamic driving force is larger for the para isomers (i.e., **p1CN** > **m1CN** and **p1Me** > **m1Me**). However, only two of them are TICT forming (i.e., **p1CN** and **m1Me**), indicating that the torsional processes in the other two isomers (i.e., **m1CN** and **p1Me**) are much slower than the decay processes of fluorescence and photoisomerization. For aminostilbenes **1CN**, the TICT state has an opposite charge-transfer direction from the PICT state, and thus, facile charge redistribution is required for initiating the changes in nuclear coordinate and the reorientation of the solvent dipoles. The poor charge-redistribution ability through the *m*-Ph bridge in **m1CN** accounts for the slow TICT-forming process. On the other hand, the charge-transfer direction is the same for the PICT and TICT states of **1Me**, and thus, the TICT-forming propensity mainly depends on the bonding character of the PICT state. The strong resonance-induced quinoidal character in the PICT state of **p1Me** disfavors the torsion of the stilbenyl−anilino C−N bond toward TICT but favors the torsion of the C=C bond for

photoisomerization. In addition, the *p*-Ph linker allows fast charge recombination in the PICT state, which facilitates the fluorescence decay. Although the driving force toward the TICT state is smaller for **m1Me** vs **p1Me**, the meta conjugation in **m1Me** results in a weaker quinoidal character and a slower charge-recombination process in its PICT state, making the single-bond torsion a competitive decay process. A slow reaction rate could also interpret the negligible TICT formation for aminostilbene DCS and aminobenzonitrile 3DMABN. Our results have provided insights not only into the kinetic aspects of the TICT model but also into the meta vs para conjugation effects on the nature of ICT states. Since the phenomenon of meta vs para isomer-dependent photochemical reactions (e.g., solvolysis,[38] trans−cis photoisomerization,[39] and excited-state proton transfer[40]) is often termed the "meta effect",[41] our results also reveal a new type of meta effect in the photochemistry.

Experimental Section

Materials. Solvents for spectra and quantum yield measurements were HPLC grade and used as received. THF was dried by sodium metal and distilled before use. All other solvents for spectra and quantum yield measurements were HPLC grade and used as received. Aminostilbenes **m1** and diarylamines CNDPAs were prepared by palladium-catalyzed amination reactions[42] between *trans*-3-bromostilbene or 4-bromobenzonitrile and the corresponding commercially available arylamines.[30] The synthesis of ring-bridged compounds **m2Me**, **m2OM**, **m3CN**, and CNDPAB also followed the same strategies previously reported for the para isomers.[30−32] All new compounds were identified by ^{1}H NMR, ^{13}C NMR, MS, IR, and/or elemental analysis. The reaction schemes and characterization data are provided as Supporting Information.

Methods. Electronic spectra were recorded at room temperature (23 ± 1 °C). UV−visible spectra were measured on a Cary300 double-beam spectrophotometer. Fluorescence spectra were recorded on a PTI QuantaMaster C-60 spectrometer and corrected for the response of the detector. The optical density (OD) of all solutions was about 0.1 at the wavelength of excitation. A N_2-bubbled solution of phenanthrene (Φ_f = 0.13 in cyclohexane)[43] was used as a standard for the fluorescence quantum yield determinations of compounds under N_2-bubbled solutions with solvent refractive index correction. An error of 10% is estimated for the fluorescence quantum yields. Fluorescence decays were also measured at room temperature by the Edinburgh FLS920 spectrometer with a gated hydrogen arc lamp using a scatter solution to profile the instrument response function. The goodness of the nonlinear least-squares fit was judged by the reduced χ^2 value (<1.2 in all cases), randomness of the residuals, and autocorrelation function. Quantum yields of photoisomerization were measured on optically dense N_2-bubbled solutions (10^{-3} M) at 313 nm using a 75-W Xe arc lamp and monochromator. *trans*-Stilbene was used as a reference standard (Φ_{tc} = 0.50 in hexane).[44] The extent of photoisomerization (<10%) was determined using HPLC analysis (Waters 600 Controller and 996 photodiode array detector, Thermo APS-2 Hypersil, heptane and ethyl acetate mixed solvent) without back-reaction corrections. The reproducibility error was <10% of the average. AM1 and DFT calculations were performed on a PC cluster using the algorithms supplied with the package of Gaussian 03 Revision B.02, a product of Gaussian Inc.[45]

Supporting Information Available: Detailed synthetic schemes and characterization data for new compounds, dual fluorescence decay times for **m1Me** and **m1OM**, solvatofluorochromic plots for **m1-m3** and CNDPAs, absorption and fluorescence spectra for **m2Me**, **m2OM**, and **m3CN**, DFT-optimized ground-state structures and energies for the meta and para isomers of **1CN** and **1Me**, detailed accounts of the energy diagrams for CNDPA, **1CN** and **1Me**, and complete ref 45 (PDF). This material is available free of charge via the Internet at http://pubs.acs.org.

(38) Dichiarante, V.; Dondi, D.; Protti, S.; Fagnoni, M.; Albini, A. *J. Am. Chem. Soc.* **2007**, *129*, 5605−5611 and references cited therein.
(39) Lewis, F. D.; Yang, J.-S. *J. Am. Chem. Soc.* **1997**, *119*, 3834−3835.
(40) (a) Lewis, F. D.; Crompton, E. M. *J. Am. Chem. Soc.* **2003**, *125*, 4044−4045. (b) Crompton, E. M.; Lewis, F. D. *Photochem. Photobiol. Sci.* **2004**, *3*, 660−668.
(41) (a) Zimmerman, H. E. *J. Am. Chem. Soc.* **1995**, *117*, 8988−8991. (b) Zimmerman, H. E. *J. Phys. Chem. A* **1998**, *102*, 5616−5621.
(42) Old, D. W.; Harris, M. C.; Buchwald, S. L. *Org. Lett.* **2000**, *2*, 1403−1406.

(43) Berlman, I. B. *Handbook of Fluorescence Spectra of Aromatic Molecules*, 2nd ed.; Academic Press: New York, 1971.
(44) Malkin, S.; Fischer, E. *J. Phys. Chem.* **1964**, *68*, 1153−1163.
(45) Frisch, M. J. et al. *Gaussian 03*, revision B.03; Gausian, Inc.; Pittsburgh, PA, 2003; full reference given in the Supporting Information.